IEEE Access
Multidisciplinary ⋮ Rapid Review ⋮ Open Access Journal

Received 22 December 2023, accepted 7 February 2024, date of publication 12 March 2024, date of current version 4 June 2024.

Digital Object Identifier 10.1109/ACCESS.2024.3376520

RESEARCH ARTICLE

A Novel Model Based on Spatio-Temporal Dilated ConvLSTM Networks for Indian Ocean Dipole Forecasting Using Multi-Source Global Sea Surface Temperature and Heat Content Data

MANVENDRA JANMAIJAYA[1], (Graduate Student Member, IEEE), MANSI JANMAIJAYA[2], AND PRANAB K. MUHURI[1], (Senior Member, IEEE)

[1]Department of Computer Science, South Asian University, New Delhi 110068, India
[2]Department of Geography, K. G. K. College, Moradabad, Uttar Pradesh 244001, India

Corresponding author: Pranab K. Muhuri (pranabmuhuri@cs.sau.ac.in)

ABSTRACT The Indian Ocean Dipole (IOD) is a critical coupled ocean–atmosphere oscillation system associated with significant weather anomalies in the global climate, particularly in the Indian Ocean rim countries. The paper presents a novel deep learning (DL) model, which we call the ''spatio-temporal dilated ConvLSTM (STDNet) model'', for forecasting the Dipole Mode Index (DMI) using global sea surface temperature (SST) and heat content (HC) data. The model combines the techniques of dilation and fine-tuning to learn efficiently from the training data. CMIP6 historical simulation data from 5 modeling centres for 1861–2014 is used to train the model. Furthermore, the model is fine-tuned on reanalysis data from 1871–1973. During the testing period (1982–2019), the dipole correlation coefficient (DCC) was the highest when compared with state-of-the-art dynamical North American Multi-Model Ensemble (NMME) models, a convolutional neural network (CNN) and a dilated CNN. On a lead of 12 months, the DCC is 0.40 for the CNN, 0.44 for the dilated CNN, and 0.51 for the STDNet, and all the NMME models have negative correlations. The results show that the STDNet efficiently forecasts the DMI at leads of up to 12 months. The STDNet shows results to overcome the winter predictability barrier.

INDEX TERMS Convolution, deep learning, dilation, dipole mode index, fine-tuning, Indian Ocean Dipole, winter predictability barrier.

I. INTRODUCTION

The eastern and south-eastern Australian summer bushfires and the floods in East Africa in 2019/2020 were extremely severe. They led to the loss of human life, livelihoods, forests, and biodiversity. These regions are usually theatres for the weather and climatic manifestations of a unique and inherent variability mechanism in the Indian Ocean. This air–ocean coupled dipole mode is called the Indian Ocean Dipole (IOD) [1]. A similar coupled air–atmosphere process in the Pacific Ocean called the El Niño–Southern Oscillation (ENSO) is also widely acknowledged. In addition to the dipole mode, there is an ocean-wide interannual SST variability mode in the tropical Indian Ocean wherein the sea surface temperature (SST) in the eastern and western parts of the ocean vary in harmony [2]. In contrast to it, a positive IOD event is characterised by anomalously cool SSTs in the south-eastern equatorial Indian Ocean (SEIO) (50° E–70° E, 10° S–10° N), off the coast of Java and Sumatra, and anomalous warming in the western equatorial Indian Ocean (WEIO) (90° E–110° E, 10° S–0° N); vice versa for the negative phase of the IOD. The 2019 positive IOD phase was identified as the

The associate editor coordinating the review of this manuscript and approving it for publication was Chuan Li.

strongest IOD event of the century [3]. The IOD is detected and quantified using a time-series index called the Dipole Mode Index (DMI). For an IOD phase to be classified as positive, the DMI must exceed 0.5 standard deviation for at least three consecutive months [3]. The IOD results in significant temperature and rain variability, particularly in the Indian Ocean rim countries, such as India [5], Africa [6], and Australia [7].

The IOD exhibits vital characteristics that are critical to its forecast and prediction. The IOD can result from a combination of intrinsic processes [1] in addition to remote influences such as ENSO [4]. A key attribute of the IOD is that its occurrence–growth–decay is phase-locked with the seasons; it appears in boreal summer (JJA), maximises in autumn (SON), and declines in winter (DJF). The interannual variability of the IOD manifests a biennial trend, i.e., an IOD event is preceded by an event of opposite polarity [1]. The IOD events are characterised by amplitude skewness, wherein the positive IOD phase is comparatively stronger than the negative equivalent, has more significant climatic impacts, and is estimated to rise substantially with global warming scenarios [5]. The IOD skewness is a result of thermocline feedback; SST responses to a positive IOD (shoaling thermocline) are more significant than those to a negative IOD (deepening feedback) [8].

The accurate prediction of IOD events advances our knowledge of climate dynamics and holds immense societal benefits [9]. The difficulty in predicting Indian Ocean SST anomalies has been attributed to various factors, namely, complex geophysical processes like interaction with the Asian Monsoon system, the remote influences of the ENSO and forcing associated with atmosphere–ocean intra-seasonal oscillations that affect the climate of the Indian Ocean region [10], weak coupling of surface temperatures with subsurface variations [11], and high event diversity [12]. The difficulties are compounded by scarce observations in the Indian Ocean region. Also, the signal-to-noise proportion is much worse in the Indian Ocean compared to the Pacific Ocean [2]. The skilful prediction of the IOD has varied from 3–4 months ahead (one season) to a few seasons ahead (for strong IOD events). The prediction skill is highly dependent on the strength of IOD events [13]. The lead time for prediction is higher for the WEIO (almost 5–6 months) compared to the SEIO (3)–4 months) because of the powerful influence of the ENSO there [10].

The predictability and persistence of the IOD exhibit significant seasonal variability [14]. The actualised predictability of the IOD is impacted by a ''winter predictability barrier'' (WPB), wherein irrespective of when the prediction is initiated, the forecast skill for the IOD drops steeply throughout the boreal winter. The WPB results from weak ocean–atmosphere coupling in the winter, leading to the rapid growth of perturbations (resulting in a winter sign reversal of the IOD index) and, therefore, a sharp drop in persistence [2]. The presence of a lesser-known summer predictability barrier in IOD predictions has also been demonstrated [15]. Thus, the potential predictability of the IOD, i.e., the maximum limit to IOD predictability, is far greater than the existing prediction skill attained so far, therefore suggesting immense scope to improve the predictability of the IOD [14], [15].

Various coupled global circulation models (CGCMs) are employed to evaluate the predictability of IOD events. These include the National Centres for Environmental Prediction (NCEP) and the Coupled Forecast System (CFS) [2], [16], as well as the Geophysical Fluid Dynamics Laboratory (GFDL) CGCM [17], the NASA season-al-to-interannual Prediction Project (NSIPP), the POAMA seasonal forecast model, the SINTEX-F model [18], the ECMWF seasonal forecast system (ECSys3), and the Community Earth System Model (CESM) [13]. Though instrumental in improving understanding of IOD events, the dynamical coupled models need to improve their skill at predicting the IOD with longer lead times. Forecast systems suffer from prediction errors, such as the simulation of systematically more considerable IOD variability [19] and peak-season amplitude [12]. An accurate simulation of the mean state of the Indian Ocean is stymied due to inadequate and erroneous model initialisation, particularly of sub-surface conditions [16], inaccurate understanding of the inner dynamics of the Indian Ocean, as well as the model's unrealistic simulation of the ENSO–IOD relationship [14]. Various strategies have been suggested to improve the prediction skill for IOD events, such as using multi-model ensembles [10] and including sub-surface ocean conditions [16]. Some studies have emphasised the value of using HC as a potential predictor for enhancing IOD predictability [20]. Also, it has been asserted that IOD predictability depends crucially on ENSO predictability.

Climate scientists have been using traditional machine-learning methods, such as non-linear Principal Component Analysis (PCA) for dimensionality reduction in multi-variate data [21], k-means clustering [22] and Artificial Neural Networks (ANNs) for forecasting rainfall, such as prediction of All India Summer Monsoon Rainfall (ISMR). Ratnam et al. [23] applied an ensemble of ANN for forecasting the IOD index, exhibiting better forecasting capability as compared to the North American Multi-Model Ensemble (NMME). However, deep learning methods have been widely applied to geoscientific datasets over the last decade.

Deep learning (DL) models have emerged as a promising tool for application to geoscientific problems. It is argued that DL models can be optimally designed to extract/learn from spatial-temporal features to improve geospatial phenomena' predictability, teleconnections modelling at varying timescales, etc [24], [25]. Forecasting in earth and climate systems is of utmost importance as an early warning system [26]. Shi et al. [27] used a convolutional long short-term memory (ConvLSTM) model for precipitation nowcasting. Shi et al. [28] proposed a self-attention joint spatio-temporal network for temperature forecasting. Zhang et al. [29] used

an LSTM for SST prediction over day–month timescales. Haghroosta [30] predicted a typhoon's wind speed using a neural network. The prediction of SST using a Deep GRU and CNN was attempted, yielding good prediction and performance [31]. Ham et al. [32] demonstrated the functionality of a CNN in skilful multi-year ENSO forecasts (with a lead time of up to 1.5 years). Attention layers in neural networks were explored in modelling SST and HC [33], and an encoder–decoder-based deep neural network was used for ENSO forecasting [34]. The geographic semantics of various latitudes and longitudes were combined with temporal attention in modelling the spatio-temporal data for long-horizon ENSO forecasting [35]. Ensemble empirical mode decomposition (EEMD) and ConvLSTM were used to forecast the North Atlantic Oscillation Index [36]. The utility of fully supervised CNNs can classify severe weather events, for example, extra-tropical storms, weather fronts, hurricanes, etc., with reasonable accuracy, as has been demonstrated. Here, a CNN resulted in a statistically significant increase in the prediction skill for hailstorm events [37]. A CNN for semi-supervised bounding box prediction was used to localise extreme weather events [38]. Vandal et al. [39] used DeepSD, a stacked super-resolution CNN (SRCNN) architecture, to statistically downscale climate variables. DL models such as CNNs are superior due to their recognition of spatial structure, weighing of parameters, self-driven feature selection, and less intensive computational demand [40]. Nonetheless, DL models face significant challenges. A fundamental limitation is the interpretability and consistency of these models with the governing laws of the earth sciences. The excessive focus on prediction accuracy often results in very complex models, which become more complicated to understand and rarely provide insights into the processes that drive the geophysical phenomenon [41]. DL models are also constrained by the availability of training data (usually limited, unlabeled, multi-sourced with diverse noise, uncertainty levels, etc.), resulting in overfitted models [26]. DL techniques, as standalone methods and in association with physical models, have been used to predict the IOD. Nevertheless, DL has not yet been used exhaustively for DMI forecasting. However, the few existing studies using DL for IOD prediction have demonstrated superior prediction skills. Liu et al. [40] used a CNN model that outperforms the North American Multi-Model Ensemble (NMME) model by exhibiting lesser sensitivity to predictability barriers and systematic errors. Similarly, Ratnam et al. [23] used an artificial neural network (ANN) that performs better than the NMME for IOD prediction. Ham et al. [32] shows that perfect modulation of two paradigms can effectively be used to fuse a new model driven by knowledge and data, also show effectively by Yu et al. [60], [61] in geochemical technologies.

This paper offers a novel DL architecture for skilful prediction of the DMI using SST and heat content (HC) data, modelled as two channels of an image. The DL models are trained on the global SST and HC domain rather than just the Indian Ocean region since it has been elucidated that IOD and ENSO predictability are intrinsically linked. This helps ensure that the models learn and integrate signals from the Pacific Ocean. In addition, the CNN model's effectiveness in predicting ENSO at an inter-annual timescale using SST and HC has already been demonstrated [32]. The study does not include an explicit heat map gradient analysis as was produced for ENSO and the IOD [40]. It includes HC only as an additional predictor, as proposed in [20], for enhancing IOD predictability. A heat map analysis can be the focus of our future study. Here, the effort is directed at developing an efficient DL model that uses data effectively. The proposed model uses convolutional LSTM and convolutional 3D, along with fine-tuning and dilation techniques, to enhance the visibility of the convolutional filters, thereby modelling the data efficiently. The proposed model, STDNet, has been experimentally investigated considering a specialised correlation coefficient, dipole correlation coefficient (DCC), and root mean square error (RMSE) and compared with traditional deep learning architecture and some dynamical models of the North American Multi-Model Ensemble (NMME). The results show that the STDNet efficiently forecasts the DMI at leads of up to 12 months. The NMME models show positive DCCs for up to 8 months, with only four months of lead on a threshold DCC of 0.5. The CNN and dilated CNN models fare better with eight months of lead on the threshold DCC. The STDNet outperforms all the models, with a 12-month lead above the threshold DCC. The STDNet shows promise to overcome the WPB. Furthermore, it has been found that the proposed STDNet is more effective than other deep learning frameworks in modelling the complex nature of the IOD.

The main contributions of the paper can be summarized as follows:

1. A novel deep learning model dilation based deep learning model with transfer learning for skilful modelling of IOD.
2. An efficient depiction of the effectiveness of the technique of dilation in geospatial data.
3. An effective transfer learning approach using reanalysis data to overcome systematic errors from CMIP.
4. The proposed model is providing skilful DMI forecast for 12 months surpassing the state-of-the-art CNN model and physical models such as NMME.

The paper is further organised into the following sections: Section II is titled Materials and Methods and includes in its subsection the mathematical formulation of the fore-casting problem, the dataset and its sources, and finally, the preliminaries. The proposed model is discussed in detail in Section III. Section IV presents the experiments and a discussion of the results. Lastly, the conclusion and future work are discussed in Section V.

II. MATERIALS AND METHODS

A. DATA

Earth system data have been abundant from a plethora of sources, such as remote sensing, in-situ observations, and model simulation outputs. The Coupled Model Intercompari-

son Project (CMIP) is the appraisal of these ''state-of-the-art'' global coupled climate (GCM) models. These models are detailed numerical/physical representations of the ocean, atmosphere, land, and cryosphere, which are coupled and interact to simulate global climate. The model output and observations share many forms of uncertainty. The models suffer from specific simulation errors. Nonetheless, these simulate large-scale regional climate and variability reasonably well.

The study utilises SST and ocean HC (in units of °C) as key variables to forecast the DMI. SST is a fundamental variable in weather prediction and atmospheric simulations. It is essential to understand the ocean's interaction with the atmosphere. HC, which mainly offers information on the ocean's upper thermal structure, is an essential parameter for initialising forecasts over seasonal-to-decadal timescales [42]. Also, the rate of ocean heat absorption due to anthropogenic climate change plays a crucial role in influencing the future SST and sea level [43]. HC (as used in the study) is the monthly averaged two-dimensional field of oceanic potential temperature ($\ominus$), which is depth-integrated from the surface to certain specified depths, described as (1). This study uses an integration depth of 0–300 m since the upper oceanic layers are considered the key source of predictability for seasonal forecasting [44].

$$\theta = \int \theta\,(x, y, z)\,dz \tag{1}$$

This study is based on historical climatic simulations from five models that participated in CMIP6 (Table 1). These models provide data for both SST and HC as used in the study. The models used in this study show only positive skewness as per the observations. Also, the models in our study show both a positive (example IPSL-CM6A-LR) and negative (example EC-Earth3) amplitude bias compared to the observations. In fact, the model results for MPI-ESM1-2-HR are very close to observations. The greater number of models used in the present study rather than a singular model helps in a better and balanced training of the deep learning models. The model output used is based on historical simulations from 1850 to 2014 (∼1.5 centuries). The present study is based on the model's native grid. For any experiment, every simulation of an ensemble of runs by a model is uniquely identified through realisation (initial conditions), initialisation (procedure, i.e., algorithms used), physics (model parameterisations), and forcing index (ripf indices). The study is based on a single ensemble member from each model, i.e., r1i1p1f1.

Ocean reanalyses utilise data assimilation techniques to aggregate diverse ocean observations and model data to estimate the ocean state. It underpins the initialisation of sub-seasonal to inter-annual forecasts and predictions of ocean dynamics [45]. The study has used Simple Ocean Data Assimilation (SODA) reanalysis data (103 years of monthly mean SST and HC) to fine-tune the deep learning models. Furthermore, the Global Ocean Data Assimilation System (GODAS) reanalysis data was used for model validation. However, a cooling period of 8 years was introduced to ensure the independence of validation from testing and fine-tuning (Table 2).

It is also of utmost importance to validate the performance of models. The forecast skills of the proposed models were compared with the suite of dynamic model forecasts from the NMME models. The NMME forecasting system is composed of a set of state-of-the-art coupled models. The NMME forecast data is accessible from 1982 to the present at different lead times. The study has utilised forecasts from six models that have continuous data, namely, CMC1-CanCM3, CMC2-CANCM4, COLA-RSMAS-CCSM3, COLA-RSMAS-CCSM4, GFDL-CM2p5-FLOR-A06, and GFDL-CM2p5-FLOR-B01 [46].

TABLE 1. CMIP6 models used in the study.

CMIP ID	Modelling Group	Resolution (in Km)	Reference
IPSL-CM6A-LR	L'Institut Pierre-Simon Laplace, France	100	Boucher et al., 2018 [47]
MPI-ESM 1-2 HR	Max Planck Institute, Germany	50	Jungclaus et al., 2019 [48]
MPI-ESM-1-2-HAM	HAMMOZ-Consortium (It is constituted by ETH Zurich and its Centre for Climate Systems Modelling (C2SM), Switzerland; Max Planck Institute, Germany; University of Oxford, UK; Finnish Meteorological Institute, Finland; Leibniz Institute for Tropospheric Research, Germany; Forschungszentrum Julich, Germany.)	250	Neubauer et al., 2019 [49]
EC-Earth3	EC-Earth Consortium, Europe	100	EC-Earth Consortium 2019 [50]
CMCC-CM2-SR5	Centro Euro-Mediterraneo per I Cambiamenti Climatici, Italy	100	Lovato and Peano, 2020 [51]

TABLE 2. Reanalysis data and testing data used in the study.

Data	Institution	Resolution	Reference
GODAS	NOAA NCEP	1 × 1°/3°	Behringer, 2007 [52]
SODA	University of Maryland/Texas A&M University	0.4 × 1°/4°	Carton and Giese, 2008 [53]
OISST	NOAA	1° × 1°	Reynolds et al., 2002 [54]

B. FORMULATION OF THE DMI FORECAST PROBLEM

The paper architects ConvLSTM and Dilated-CNNs and proposes a new and unique STDNet model for the forecasting

of the DMI. The main goal of IOD forecasting is to use historical and reanalysed SST and HC data frames to forecast the DMI of the region of interest (ROI). Suppose our ROI is denoted by a M × N grid, where M and N are latitudes and longitudes, respectively, and each grid point represents two observations (SST and HC). Therefore, we can represent a frame of observation as $X \in R^{2\times M\times N}$, where R is the field of the observed features, and K $\in R$, where K is the DMI. The periodic observation can be represented as a sequence of tensors: $X_1, X_2, X_3, \ldots\ldots.., X_t$. Now, as the IOD is seasonal in nature, the spatio-temporal DMI forecasting problem to predict the DMI given three months of observations can be determined by (2):

$$\widehat{K} = f\left(X_{t+l} \mid X_t, X_{t-1}, X_{t-2}\right) \tag{2}$$

where K is the DMI, X_{t+l} is the predicted frame, and $l$is the lead time.

The historical simulations of SST and HC from CMIP6 climate modelling groups have been used to train the prediction models (Table 1). The study applies the fine-tuning technique, using the SODA data to train the models optimally. The prediction models are, thereafter, validated with the GODAS data. The data covers the area of 0°–360° E and 55° S–60° N. As the data from the three sources are at different resolutions (Table 2), they were further interpolated into a 72 × 24 matrix using the Climate Data Operators (CDO) bilinear interpolation tool. This allowed consistency amongst model spatial grids as well as promoted computational efficiency without losing essential data. The CDO and National Centre for Atmospheric Research (NCAR) Command Library (NCL) were used for the data pre-processing. The anomalies were calculated as the monthly deviation from the base climatology. The DMI labels were calculated as the difference in SST between the EEIO and the WEIO. The variables/predictors for SST and HC are modelled as two channels of an image. Rather than giving the model six different frames of SST and HC, three frames of these two-channel images are fed to the model as inputs. The idea behind the formulation is to preserve the pixel-level relationship between the two variables spatially.

C. PRELIMINARIES

1) CONVOLUTIONAL LAYER

A convolution layer was proposed by LeCun et al. [55], where CNN was proposed for image processing tasks. The purpose of a convolutional layer is to obtain meaningful features from the input image, which can further be used for classification, segmentation, or other image-processing tasks. The layer works by applying a set of filters (kernels) to the input image and producing a set of output feature maps. Each filter is a small matrix composed of weights that slides over the input, performing element-wise multiplication and summing up the results to produce a single value in the output feature map. A con-volution layer can extract different feature types from different locations using multiple filters. The output feature map of a single filter at a particular location in the input image can be calculated as follows:

$$O_{i,j} = \sum_{m=0}^{k-1}\sum_{n=0}^{k-1} I_{i+m,j+n} \times W_{m,n} \tag{3}$$

where $O_{i,j}$ is the value of the output feature map at location (i, j), $I_{i+m,j+n}$ is the value of the input image at location $(i+m, j+n)$, $W_{m,n}$ is the weight of the filter at position (m, n), and k is the size of the filter.

For a sequence of images, such as videos, Ji et al. [56] proposed 3D convolutional neural networks. In a 3D convolution layer, a set of 3D filters is applied to the input data as follows:

$$O_{i,j} = \sum_{m=0}^{k-1}\sum_{n=0}^{k-1}\sum_{p=0}^{k-1} I_{i+m,j+n,k+p} \times W_{m,n,p} \tag{4}$$

where $O_{i,j,k}$ is the value of the output feature map at location (I, j, k), $I_{i+m,j+n,k+p}$ is the value of the input image at location $(i+m, j+n, k+p)$, $W_{m,n,p}$ is the weight of the filter at position (m, n, p), and k is the size of the filter in each dimension.

2) ConvLSTM

ConvLSTM was introduced by Shi et al. [27] to counter the drawbacks of FC-LSTM. Primarily, conventional FC-LSTMs flatten the inputs to a single dimension, thereby losing all the spatial features. ConvLSTM captures the spatial features of 3D input data by re-placing matrix multiplication with a convolutional operator at each gate in the LSTM cell. In other words, the future state of a cell in a grid can be determined by ConvLSTM by using the inputs and past states of its local neighbours, which can be achieved by using convolution operators for state-to-state and input-to-state operators. The basic formulations of ConvLSTM are given as (5) – (10):

$$i_t = \sigma\left(W_{xi} \circledast X_t + W_{hi} \circledast H_{t-1} + W_{ci} \diamond C_{t-1} + b_i\right) \tag{5}$$
$$f_t = \sigma\left(W_{xf} \circledast X_t + W_{hf} \circledast H_{t-1} + W_{cf} \diamond C_{t-1} + b_f\right) \tag{6}$$
$$\tilde{C}_t = tanh\left(W_{xc} \circledast X_t + W_{hc} \circledast H_{t-1} + b_c\right) \tag{7}$$
$$C_t = f_t \diamond C_{t-1} + i_t \diamond \tilde{C}_t \tag{8}$$
$$o_t = \sigma\left(W_{xo} \circledast X_t + W_{ho} \circledast H_{t-1} + W_{co} \diamond C_t + b_o\right) \tag{9}$$
$$H_t = o_t \diamond tanh\left(C_t\right) \tag{10}$$

where σ denotes the sigmoid function, $\circledast$ represents the convolutional operator, and $\diamond$ represents the dot product. X_t are the inputs, C_t are the cell outputs, H_t are the hidden states, and i_t, f_t, o_t are the input, forget, and output gates, respectively.

3) DILATED ConvLSTM

The size of the region in the input that is used to produce the feature is known as the receptive field (RF). Therefore, a larger receptive field will make certain that no important information is omitted. Dilation is applied to local operations like convolution; therefore, we introduce dilation to the convolution operation in ConvLSTM. The dilated convolution operation will learn features from a larger receptive field.

A dilated convolution operation is performed by introducing "holes" between pixels, which are basically gaps or zeros between the values of the kernel. The number of gaps is governed by the dilation rate, r. Figure 1 shows the convolutional kernel with different dilation rates. For a kernel of size k, the size of the dilated kernel will be as follows:

$$k_r = k + (k-1) \times (r-1) \tag{11}$$

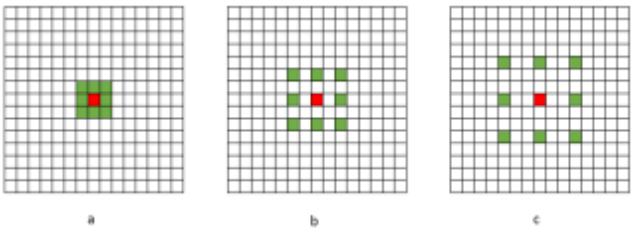

FIGURE 1. Dilated convolution kernels with dilation rates of (a) 1, (b) 2, and (c) 3.

The dilation operation in a convolution can be stated as:

$$Y = X \tilde{\circledast} W_{k_r} \tag{12}$$

where Y is the output, X is the input, $\tilde{\circledast}$ is the dilated convolution operator, and W_{k_r} is the kernel. Thus, in the ConvLSTM equations, the convolution operator can be replaced by the dilated convolution as operator shown in (13)–(18).

$$i_t = \sigma\left(W_{xi} \circledast \widetilde{X_t} + W_{hi} \circledast \widetilde{H_{t-1}} + W_{ci} \diamond C_{t-1} + b_i\right) \tag{13}$$

$$f_t = \sigma\left(W_{xf} \widetilde{\circledast} X_t + W_{hf} \widetilde{\circledast} H_{t-1} + W_{cf} \diamond C_{t-1} + b_f\right) \tag{14}$$

$$\tilde{C}_t = tanh\left(W_{xc} \widetilde{\circledast} X_t + W_{hc} \widetilde{\circledast} H_{t-1} + b_c\right) \tag{15}$$

$$C_t = f_t \diamond C_{t-1} + i_t \diamond \tilde{C}_t \tag{16}$$

$$o_t = \sigma\left(W_{xo} \widetilde{\circledast} X_t + W_{ho} \widetilde{\circledast} H_{t-1} + W_{co} \diamond C_t + b_o\right) \tag{17}$$

$$H_t = o_t \diamond tanh\left(C_t\right) \tag{18}$$

III. PROPOSED DMI FORECAST MODEL

In this section, we discuss our proposed STDNet model for forecasting the DMI in detail. The study uses SST and HC for 3 consecutive months, i.e., St−2, St−1, St, as the predictors. For DMI forecasting, we have defined the lead months as the number of intervening months between the latest month for which observation data are used for the forecast and the mean of the three-month forecast target season.

The STDNet model shown in Figure 2 is composed of three staged ConvLSTM blocks called Dilated ConvLSTM (DCL) blocks. The dilation rates of the three DCL blocks are set at 1, 2, and 3. This was chosen to ensure that the spatial features are extracted at multiple levels. For the first block with a dilation rate of 1, it performs as a standard convolution operation; therefore, for a filter size of k = 3, the receptive field $k\_r = 3$, as per (11). With a dilation rate of 2 and $k = 3$, the receptive field $k\_r = 5$. Similarly, for the third block, the dilation rate is 3, and thus, the receptive filed $k\_r = 7$. This setting ensures that spatial signals from different levels are captured in a serial way. A DCL block has two maximum pooling layers and batch normalisation with dropout between them. The filter size of maxpool layers is set at 2, which extracts the maximum values from a 2 × 2 grid. The batch normalisation layer standardises the activations by first determining the mean and the variance, as shown in (19) - (21).

$$\mu = \frac{1}{n}\sum_i Z^i \tag{19}$$

$$\sigma^2 = \frac{1}{n}\sum_i \left(Z^i - \mu\right)^2 \tag{20}$$

$$Z^{(i)}_{norm} = \frac{Z^{(i)} - \mu}{\sqrt{\sigma^2 - \epsilon}} \tag{21}$$

Furthermore, a CNN3D convolves over the entire time sequence features from the DCL blocks for spatial features to produce the predicted frame. Two fully connected dense layers and a single output layer (the predictand) provide the final predicted DMI value. The input images were convolved with an 8 × 4 convolutional kernel/filter in the first convolutional process and subsequently with a 4 × 2 convolutional kernel. The value of the convolutional matrix is specified by iteration to minimise the cost function (defined as the average squared difference between the predicted and true values).

The convolutional process of CNN extracts key local features from multi-dimensional global geospatial data. It calculates the dot products between the convolutional filter and input data. The output of the convolutional process is a feature layer, which is further flattened to a vector. A fully connected layer is then used to predict the final DMI value.

IV. RESULTS AND DISCUSSION

The study predicts the DMI (predictand) using three running successive-month SST and HC anomaly maps (predictors) over the Indian Ocean region. The analysis investigates the reliability of DL models that use multi-dimensional geographical variables to forecast a uni-dimensional index. The predictors SST anomaly and HC maps are modelled as two different channels of a month, and a further three consecutive months of data are provided as input to the STDNet model to forecast the DMI at a particular lead. The lead time refers to the difference between the middle of the target season and the last observed data. The model is described in Figure 3.

DL requires an abundance of data for training; therefore, to counter this limitation (as there are only 12 spatio-temporal data points for each year), the transfer learning (TL) approach has been utilised. The STDNet model is first trained with the historical simulation datasets (CMIP6), and then the model is trained to find the suboptimal weights. Furthermore, the model is initialised using these suboptimal weights and further trained with the SODA dataset. For training, the learning rate was set to 0.005, whereas for the fine-tuning phase, the learning rate was fixed at 0.0005. The learning rate during the fine-tuning phase was kept low to avert overfit. For the forecast, mean squared error and the correlation skill are used

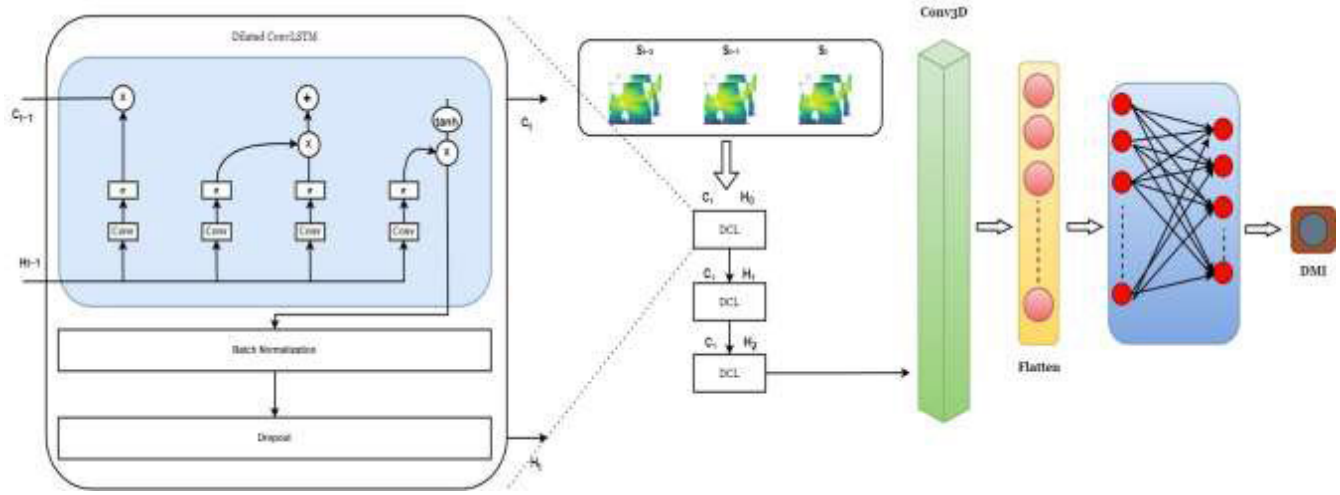

FIGURE 2. STDNet architecture.

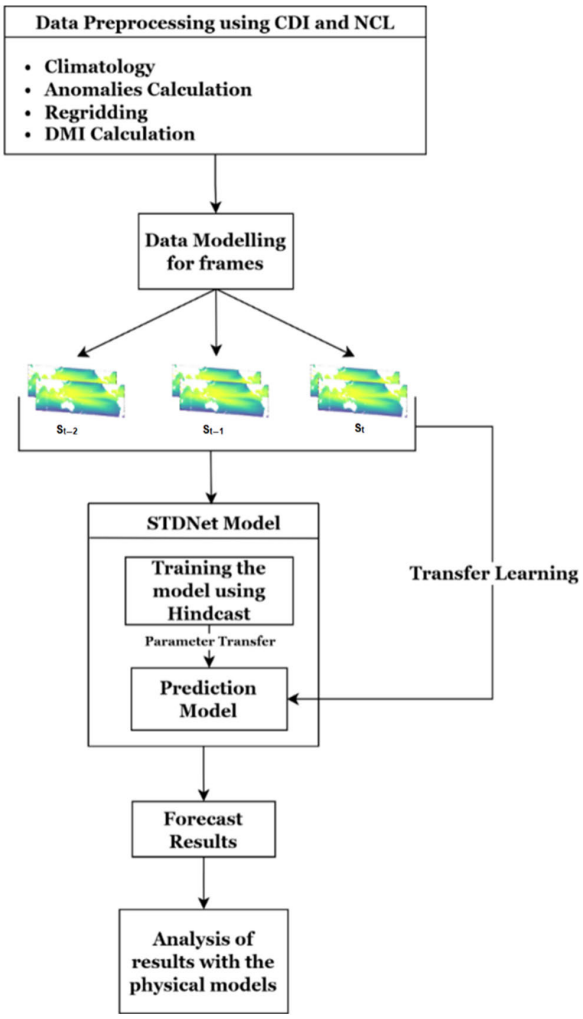

FIGURE 3. Fine-tuning model with a STDNet for DMI forecasting.

for evaluation, which are given as follows:

$$MSE = \frac{1}{n}\sum_{i=1}^{n}\left(Y_i - \hat{Y}_i\right)^2 \tag{22}$$

where N is the number of instances, Y is the ground, and Y ^_i is the predicted value. The dipole correlation coefficient (DCC) is defined as the cost function:

$$DCC_l = \sum_{m=1}^{12} \frac{\sum_{y=s}\left(Y_{y,m} - \bar{Y}_m\right)\left(P_{y,m,l} - \bar{P}_{m,l}\right)}{\sqrt{\sum_{y=s}^{e}\left(Y_{y,m} - \bar{Y}_m\right)^2 \sum_{y=s}^{e}\left(P_{y,m,l} - \bar{P}_m\right)^2}} \tag{23}$$

where P and Y denote the predicted and the observed values, respectively, $\bar{P}_m$ and $\bar{Y}_{m,l}$ are the climatologies with respect to l (lead months) and m (calendar month), y denotes the target forecast year, and s and e represent the validation years.

DL approaches have been explored in conjunction with the physical models for studying the domain of the IOD. Table 3 lists and compares the attempts made to forecast the IOD using deep learning models. Essentially, CNN and ConvLSTM have been shown to give promising results; however, they are only able to provide skilful predictions for up to 7 months of lead time. Different combinations of predictor variables have also been explored. Liu et al. [40] showed that SST is a very effective predictor for DMI. Sarkar et al. [58] augmented SST and wind along with 81 other atmosphere and sea parameters for IOD forecasting with a lead time of 7 months. Further attempts with LSTM, CNNs, and artificial neural networks were made. Ham et al. [32] have shown that HC is an excellent predictor for coupled ocean–atmospheric events. Therefore, this study explores the predictability of SST and HC for the DMI.

The associated correlation skill (DCC) and RMSE of the NMME models and ConvLSTM, Dilated-CNN, and STDNet models are compared (Figures 4 and 5). Herein, we consider a DCC value of 0.5 as a threshold for skilful forecasting. A decline in the forecast skill is indicated by a reduction in DCC as the lead time for the models increases. The results demonstrate that the DL models, particularly the STDNet, exhibit the highest forecasting skills. The STDNet starts off

TABLE 3. Deep learning techniques in IOD prediction.

Model	Data Purpose	Variables	Time Period	Lead Time
Long short-term memory (LSTM) with machine learning (random decision forest tree) model for index prediction [58]	Feature extraction	DMI, SST, 800 and 200 hPa geopotential height anomalies, u-v wind component, air temperature, sea level pressure, normalised ISMR anomalies, and equatorial OLR	1980–2018, except for the DMI (1950–2018)	Five months
CNN in conjunction with a physical-empirical (PE) model [57]	20 CMIP6 models for training	Sea surface height (SSH), sea ice concentration (SIC)	1871–1982	3–4 months
Artificial neural network with a jackknife approach and bootstrap method [23]	Identification of attributes by correlation analysis	SST, 850 hPa and 200 hPa geopotential height anomalies	1949–2018	May–November Index from February–April initialisation conditions
CNN [40]	Extended Reconstructed SST (ERSST) v5 for CNN training	Three successive months of SST anomalies	1854–1989	Seven months
ConvLSTM [59]	Past 125 months of data from NCEP for training	81 parameters of atmosphere, subsea, sea surface, and wind field	1861–2019	Next seven months (June to December)
Proposed STDNet	CMIP6 for training, SODA for fine-tuning	Three successive months of SST anomalies and HC data	1861–2019	12 months

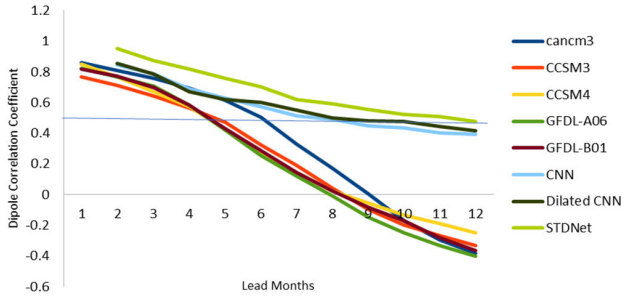

FIGURE 4. DCC comparison with lead times.

with very high skill, varying between 0.9 and 0.8 for a lead period of up to 4 months. It possesses the skill (DCC of 0.6) to forecast the DMI with a lead time of 8 months. Thereafter, the model predicts the DMI with a moderate skill of ∼0.5 up to leads of 12 months. The forecasting skills of ConvLSTM and Dilated-CNN mimic each other closely. These models can forecast the DMI with a skill of 0.5 and a lead time of 8 months. This is marginally lower than that of the STDNet. After eight months, the skills drop to 0.41 for a 4-month lead period.

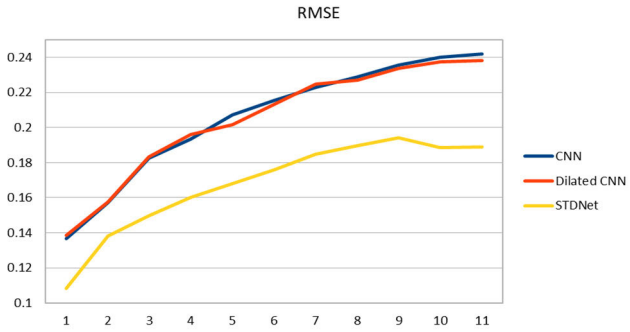

FIGURE 5. RMSE comparison with lead times.

It is noteworthy that the ability to forecast the DMI drops rather steeply for the NMME dynamic models, particularly after a lead forecast of up to 4 months. On the other hand, the models proposed in this paper maintain forecasting fidelity for up to a year, wherein the skill decreases gradually as the lead time increases. This clearly demonstrates that the deep learning models, and specifically the STDNet, outperform the NMME dynamic models for forecasting the DMI. Seasonal phase locking is a defining feature of the IOD. Subsequently, the forecast skill of the DMI varies with the seasons. However, as discussed in Section I, the predictability of the IOD is dampened by the existence of the WPB, wherein the forecasting skill diminishes rapidly across the winter season. In addition, there is a late boreal spring/early summer predictability barrier wherein the predictive skill for the starting months before May is very constrained.

The seasonal forecast skill of the DL and NMME models is evaluated by calculating the DCC between the ensemble mean anomaly and the observed anomaly for each of the 12 months of the hindcast forecast as a function of the initialising month. Seasonal forecasts yielding correlation values greater than 0.5 are deemed skilled. The seasons are defined as consecutive running months, such as boreal autumn, which is September-October-November (SON); winter, which is December-January-February (DJF); spring, which is March-April-May (MAM); and summer, which is June-July-August (JJA). Here, the study compared the DMI seasonal forecast skill from the ConvLSTM, Dilated-CNN, and STDNet models with the ensemble forecasts from the state-of-the-art NMME models. It is evident from Figure 6 that the ConvLSTM and, mainly, the STDNet models are much less affected by the WPB and SPB.

The heatmap analysis of the seasonal forecast signal is shown in Figure 6. The marked cells have a DCC greater than 0.5. The predictive skill for the DMI in boreal autumn (SON) is limited to 3–4 months (∼1 season) in the NMME models. The skill thereafter diminishes rapidly (OND and NDJ seasons). However, predictability recovers in the late winter. On the other hand, the models used in our study have redictive skills for the DMI for as long as 6–7 lead months for the SON season. Also, there is no decline in the predictive skill thereafter. The STDNet model showcases

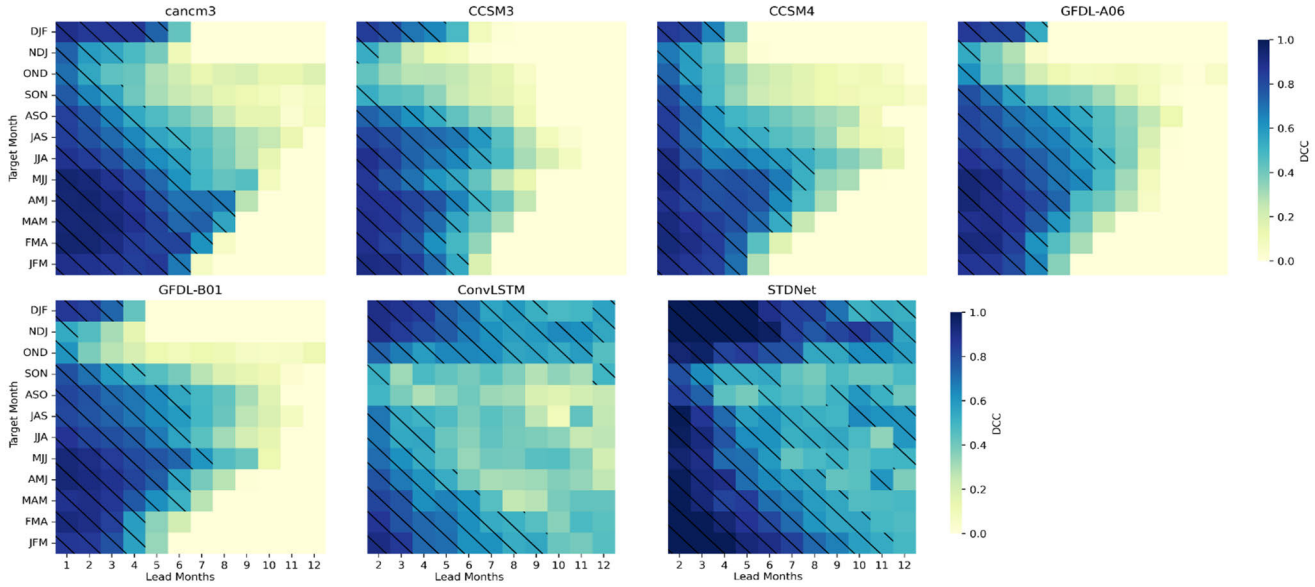

FIGURE 6. Heatmap analysis of forecast signals.

high skill through the boreal winter, with lead months as high as 12 months.

The NMME models can predict SST variability for boreal spring (MAM) with lead months varying from 5–6 months, whereas the DL models have the skill to predict with 8–9 months of lead. Hence, the models demonstrate the potential to significantly overcome the SPB as well (Figure 6). It is important to note here that the DMI sign in the boreal spring is opposite to the preceding boreal fall sign. It can, thus, be concluded that the better performance of the DL models compared to NMME models in DMI prediction is largely due to their ability to overcome the loss of skill during winter and late spring/early summer by weakening the WPB and SPB, respectively.

The sub-surface HC is an effective variable for identifying the precursors and underlying physical processes for the IOD, which significantly enhances the predictive skill of our models. It has been pointed out and reiterated by Wajsowicz [2] that HC enables predictive skill to return if there is a loss of skill in forecasting weak SST signals during boreal winter (particularly December) and again in boreal summer (in May).

V. CONCLUSION

This paper has proposed a novel deep learning model, STDNet, for forecasting the DMI for leads ranging from one month to twelve months and has been assessed in comparison with other competitor models (CNN, Dilated-CNN) and dynamic NMME physical models. Of these models, the STDNet model has demonstrated the highest skill in forecasting the DMI, with lead times as high as twelve months. It is quite evident, in comparison with other DL models, that the STDNet is a highly sophisticated model with abundant training and fine-tuning exercises. The model has demonstrated efficacy in overcoming the seasonal predictability barriers often encountered in IOD prediction. The analysis of observational and reanalysis datasets in the present study has demonstrated that the advancement in the prediction skill of the deep learning model is due to the sub-surface signals, particularly the HC data averaged over the upper layers of the ocean. The HC holds cues and memory to identify and understand the key underlying physical processes. Also, the study focuses on both the eastern and western poles of the tropical IOD rather than focusing on the predictability of SST anomalies at each pole in isolation. For a lead of twelve months, where the dynamical NMME models have shown a negative DCC, the CNN and Dilated-CNN have a 0.40 and 0.44 DCC, respectively, and the STDNet has a significant DCC of 0.51.

The proposed STDNet model holds significant promise for multi-year prediction of IOD events in the future. Future research may also extend the study to analyse the predictability of the IOD in association with ENSO. The existence of the IOD as a physical entity and its independence/dependence from ENSO has been questioned and widely studied. Also, more observational and reanalysis data, such as equatorial winds and HC in the middle of the ocean (up to 700 m in depth), could be integrated to improve the prediction skills of the STDNet and other deep learning models. SST, along with HC, has been shown to be good predictors for the DMI. However, the predictive power of the STDNet with only the SST can be compared with the present HC-enhanced predictor. Moreover, examining how the model performs without fine-tuning would bring about its raw predictive strengths. Another exciting avenue would be to assess how well our model can predict the DMI as simulated by CMIP6 using cross-validation techniques. This would help us understand our model's ability to handle complex climate simulations.

Finally, a key question remains about the dilation step in our model's architecture: What if we skip it? Exploring this could uncover whether this step is essential for capturing the nuances of temporal changes or if we can maintain model efficiency without it. These areas offer promising directions for enhancing our understanding and capabilities in climate forecasting with deep learning. Nevertheless, the study demonstrates that deep learning techniques hold immense potential to improve the predictability of geophysical phenomena in addition to dynamical physical models.

REFERENCES

[1] N. H. Saji, B. N. Goswami, P. N. Vinayachandran, and T. Yamagata, "A dipole mode in the tropical Indian ocean," *Nature*, vol. 401, no. 6751, pp. 360–363, Sep. 1999, doi: 10.1038/43854.

[2] R. C. Wajsowicz, "Seasonal-to-interannual forecasting of tropical Indian ocean sea surface temperature anomalies: Potential predictability and barriers," *J. Climate*, vol. 20, no. 13, pp. 3320–3343, Jul. 2007, doi: 10.1175/jcli4162.1.

[3] W. Shi and M. Wang, "A biological Indian Ocean Dipole event in 2019," *Sci. Rep.*, vol. 11, no. 1, p. 2452, Jan. 2021, doi: 10.1038/s41598-021-81410-5.

[4] Q. Song, G. A. Vecchi, and A. J. Rosati, "Indian ocean variability in the GFDL coupled climate model," *J. Climate*, vol. 20, no. 13, pp. 2895–2916, Jul. 2007, doi: 10.1175/jcli4159.1.

[5] K. Ashok, Z. Guan, and T. Yamagata, "Impact of the Indian ocean dipole on the relationship between the Indian monsoon rainfall and ENSO," *Geophys. Res. Lett.*, vol. 28, no. 23, pp. 4499–4502, Dec. 2001, doi: 10.1029/2001gl013294.

[6] H. S. Endris, C. Lennard, B. Hewitson, A. Dosio, G. Nikulin, and G. A. Artan, "Future changes in rainfall associated with ENSO, IOD and changes in the mean state over Eastern Africa," *Climate Dyn.*, vol. 52, nos. 3–4, pp. 2029–2053, May 2018, doi: 10.1007/s00382-018-4239-7.

[7] G. Wang and W. Cai, "Two-year consecutive concurrences of positive Indian Ocean Dipole and Central Pacific El Niño preconditioned the 2019/2020 Australian 'black summer' bushfires," *Geosci. Lett.*, vol. 7, no. 1, pp. 7–19, Nov. 2020, doi: 10.1186/s40562-020-00168-2.

[8] B. Ng, W. Cai, and K. Walsh, "The role of the SST-thermocline relationship in Indian Ocean Dipole skewness and its response to global warming," *Sci. Rep.*, vol. 4, no. 1, p. 6034, Aug. 2014, doi: 10.1038/srep06034.

[9] C. Yuan and T. Yamagata, "Impacts of IOD, ENSO and ENSO Modoki on the Australian winter wheat yields in recent decades," *Sci. Rep.*, vol. 5, no. 1, p. 17252, Nov. 2015, doi: 10.1038/srep17252.

[10] J.-J. Luo, S. Masson, S. Behera, and T. Yamagata, "Experimental forecasts of the Indian ocean dipole using a coupled OAGCM," *J. Climate*, vol. 20, no. 10, pp. 2178–2190, May 2007, doi: 10.1175/jcli4132.1.

[11] M. Zhao and H. H. Hendon, "Representation and prediction of the Indian ocean dipole in the POAMA seasonal forecast model," *Quart. J. Roy. Meteorolog. Soc.*, vol. 135, no. 639, pp. 337–352, Jan. 2009, doi: 10.1002/qj.370.

[12] C. Tanizaki, T. Tozuka, T. Doi, and T. Yamagata, "Relative importance of the processes contributing to the development of SST anomalies in the eastern pole of the Indian ocean dipole and its implication for predictability," *Climate Dyn.*, vol. 49, no. 4, pp. 1289–1304, Oct. 2016, doi: 10.1007/s00382-016-3382-2.

[13] X. Song, Y. Tang, T. Liu, and X. Li, "Predictability of Indian Ocean Dipole over 138 years using a CESM Ensemble?Prediction system," *J. Geophys. Res., Oceans*, vol. 127, no. 3, Feb. 2022, Art. no. e2021JC018210, doi: 10.1029/2021jc018210.

[14] H. Liu, Y. Tang, D. Chen, and T. Lian, "Predictability of the Indian ocean dipole in the coupled models," *Climate Dyn.*, vol. 48, nos. 5–6, pp. 2005–2024, Jun. 2016, doi: 10.1007/s00382-016-3187-3.

[15] D. Liu, W. Duan, R. Feng, and Y. Tang, "Summer predictability barrier of Indian ocean dipole events and corresponding error growth dynamics," *J. Geophys. Res., Oceans*, vol. 123, no. 5, pp. 3635–3650, May 2018, doi: 10.1029/2017jc013739.

[16] L. Shi, H. H. Hendon, O. Alves, J.-J. Luo, M. Balmaseda, and D. Anderson, "How predictable is the Indian ocean dipole?" *Monthly Weather Rev.*, vol. 140, no. 12, pp. 3867–3884, Dec. 2012, doi: 10.1175/mwr-d-12-00001.1.

[17] Q. Song, G. A. Vecchi, and A. Rosati, "Predictability of the Indian Ocean sea surface temperature anomalies in the GFDL coupled model," *Geophys. Res. Lett.*, vol. 35, no. 2, Jan. 2008, Art. no. L02701, doi: 10.1029/2007gl031966.

[18] T. Doi, A. Storto, S. K. Behera, A. Navarra, and T. Yamagata, "Improved prediction of the Indian ocean dipole mode by use of subsurface ocean observations," *J. Climate*, vol. 30, no. 19, pp. 7953–7970, Sep. 2017, doi: 10.1175/jcli-d-16-0915.1.

[19] J. Luo, S. K. Behera, Y. Masumoto, H. Sakuma, and T. Yamagata, "Successful prediction of the consecutive IOD in 2006 and 2007," *Geophys. Res. Lett.*, vol. 35, no. 14, Mar. 2008, Art. no. L14S02, doi: 10.1029/2007gl032793.

[20] M. Liu, M. J. McPhaden, H. Ren, M. Balmaseda, and R. Wang, "Oceanic heat content as a predictor of the Indian Ocean Dipole," *J. Geophys. Res., Oceans*, vol. 127, no. 12, Dec. 2022, Art. no. e2022JC018896, doi: 10.1029/2022jc018896.

[21] A. H. Monahan, "Nonlinear principal component analysis: Tropical Indo–Pacific sea surface temperature and sea level pressure," *J. Climate*, vol. 14, no. 2, pp. 219–233, Jan. 2001, doi: 10.1175/1520-0442(2001)013<0219:NPCATI>2.0.CO;2.

[22] K. Steinhaeuser, N. V. Chawla, and A. R. Ganguly, "Comparing predictive power in climate data: Clustering matters," in *Proc. Int. Symp. Spatial Temporal Databases*, in Lecture Notes in Computer Science, 2011, pp. 39–55, doi: 10.1007/978-3-642-22922-0_4.

[23] J. V. Ratnam, H. A. Dijkstra, and S. K. Behera, "A machine learning based prediction system for the Indian Ocean Dipole," *Sci. Rep.*, vol. 10, no. 1, p. 284, Jan. 2020, doi: 10.1038/s41598-019-57162-8.

[24] S. Kumar and P. K. Muhuri, "A novel GDP prediction technique based on transfer learning using CO_2 emission dataset," *Appl. Energy*, vol. 253, Nov. 2019, Art. no. 113476, doi: 10.1016/j.apenergy.2019.113476.

[25] S. Kumar, A. K. Shukla, and P. K. Muhuri, "Anomaly based novel multi-source unsupervised transfer learning approach for carbon emission centric GDP prediction," *Comput. Ind.*, vol. 126, Apr. 2021, Art. no. 103396, doi: 10.1016/j.compind.2021.103396.

[26] M. Reichstein, G. Camps-Valls, B. Stevens, M. Jung, J. Denzler, N. Carvalhais, and F. Prabhat, "Deep learning and process understanding for data-driven Earth system science," *Nature*, vol. 566, no. 7743, pp. 195–204, Feb. 2019, doi: 10.1038/s41586-019-0912-1.

[27] X. Shi, Z. Chen, H. Wang, D.-Y. Yeung, W.-K. Wong, and W.-C. Woo, "Convolutional LSTM network: A machine learning approach for precipitation nowcasting," 2015, *arXiv:1506.04214*.

[28] L. Shi, N. Liang, X. Xu, T. Li, and Z. Zhang, "SA-JSTN: Self-attention joint spatiotemporal network for temperature forecasting," *IEEE J. Sel. Topics Appl. Earth Observ. Remote Sens.*, vol. 14, pp. 9475–9485, 2021, doi: 10.1109/JSTARS.2021.3112131.

[29] Q. Zhang, H. Wang, J. Dong, G. Zhong, and X. Sun, "Prediction of sea surface temperature using long short-term memory," *IEEE Geosci. Remote Sens. Lett.*, vol. 14, no. 10, pp. 1745–1749, Oct. 2017, doi: 10.1109/LGRS.2017.2733548.

[30] T. Haghroosta, "Comparative study on typhoon's wind speed prediction by a neural networks model and a hydrodynamical model," *MethodsX*, vol. 6, pp. 633–640, Jan. 2019, doi: 10.1016/j.mex.2019.03.002.

[31] X. Yu, S. Shi, L. Xu, Y. Liu, Q. Miao, and M. Sun, "A novel method for sea surface temperature prediction based on deep learning," *Math. Problems Eng.*, vol. 2020, pp. 1–9, May 2020, doi: 10.1155/2020/6387173.

[32] Y.-G. Ham, J.-H. Kim, and J.-J. Luo, "Deep learning for multi-year ENSO forecasts," *Nature*, vol. 573, no. 7775, pp. 568–572, Sep. 2019, doi: 10.1038/s41586-019-1559-7.

[33] J. Kim, M. S. Kwon, S. D. Kim, J. Kug, J.-G. Ryu, and J. Kim, "Spatiotemporal neural network with attention mechanism for El Niño forecasts," *Sci. Rep.*, vol. 12, no. 1, p. 7204, May 2022, doi: 10.1038/s41598-022-10839-z.

[34] X. Zhang, Y. Wang, L. Wei, J. Jiang, P. Lin, and H. Liu, "Spatiotemporal networks for ENSO forecasting with LICOM3 and remote sensing data," *Eng. Appl. Artif. Intell.*, vol. 125, Oct. 2023, Art. no. 106641, doi: 10.1016/j.engappai.2023.106641.

[35] J. Zhao, H. Luo, W. Sang, and K. Sun, "Spatiotemporal semantic network for ENSO forecasting over long time horizon," *Appl. Intell.*, vol. 53, no. 6, pp. 6464–6480, Jul. 2022, doi: 10.1007/s10489-022-03861-1.

[36] S. Yuan, X. Luo, B. Mu, J. Li, and G. Dai, "Prediction of North Atlantic oscillation index with convolutional LSTM based on ensemble empirical mode decomposition," *Atmosphere*, vol. 10, no. 5, p. 252, May 2019, doi: 10.3390/atmos10050252.

[37] D. J. Gagne II, S. E. Haupt, D. W. Nychka, and G. Thompson, "Interpretable deep learning for spatial analysis of severe hailstorms," *Monthly Weather Rev.*, vol. 147, no. 8, pp. 2827–2845, Jul. 2019, doi: 10.1175/mwr-d-18-0316.1.
[38] E. Racah, C. Beckham, T. Maharaj, S. E. Kahou, Prabhat, and C. Pal, "ExtremeWeather: A large-scale climate dataset for semi-supervised detection, localization, and understanding of extreme weather events," in *Proc. Neural Inf. Process. Syst.*, vol. 30, Jan. 2017, pp. 3402–3413. [Online]. Available: https://papers.nips.cc/paper/2017/file/519c84155964659375821f7ca576f095-Paper.pdf
[39] T. Vandal, E. Kodra, S. Ganguly, A. Michaelis, R. Nemani, and A. R. Ganguly, "DeepSD: Generating high resolution climate change projections through single image super-resolution," 2017, *arXiv:1703.03126*.
[40] J. Liu, Y. Tang, Y. Wu, T. Li, Q. Wang, and D. Chen, "Forecasting the Indian ocean dipole with deep learning techniques," *Geophys. Res. Lett.*, vol. 48, no. 20, Oct. 2021, doi: 10.1029/2021gl094407.
[41] J. H. Faghmous and V. Kumar, "A big data guide to understanding climate change: The case for theory-guided data science," *Big Data*, vol. 2, no. 3, pp. 155–163, Sep. 2014, doi: 10.1089/big.2014.0026.
[42] M. A. Balmaseda, O. J. Alves, A. Arribas, T. Awaji, D. W. Behringer, N. Ferry, Y. Fujii, T. Lee, M. Rienecker, T. Rosati, and D. Stammer, "Ocean initialization for seasonal forecasts," *Oceanography*, vol. 22, no. 3, pp. 154–159, Sep. 2009, doi: 10.5670/oceanog.2009.73.
[43] T. Kuhlbrodt and J. M. Gregory, "Ocean heat uptake and its consequences for the magnitude of sea level rise and climate change," *Geophys. Res. Lett.*, vol. 39, no. 18, Sep. 2012, Art. no. L18608, doi: 10.1029/2012gl052952.
[44] M. D. Palmer, C. D. Roberts, M. Balmaseda, Y. S. Chang, G. Chepurin, N. Ferry, Y. Fujii, S. A. Good, S. Guinehut, K. Haines, and F. Hernandez, "Ocean heat content variability and change in an ensemble of ocean reanalyses," *Climate Dyn.*, vol. 49, no. 3, pp. 909–930, Sep. 2015, doi: 10.1007/s00382-015-2801-0.
[45] A. Storto, A. Alvera-Azcárate, M. A. Balmaseda, A. Barth, M. Chevallier, F. Counillon, C. M. Domingues, M. Drevillon, Y. Drillet, G. Forget, and G. Garric, "Ocean reanalyses: Recent advances and unsolved challenges," *Frontiers Mar. Sci.*, vol. 6, p. 418, Jul. 2019, doi: 10.3389/fmars.2019.00418.
[46] B. P. Kirtman, D. Min, J. M. Infanti, J. L. Kinter, D. A. Paolino, Q. Zhang, H. Van Den Dool, S. Saha, M. P. Mendez, E. Becker, and P. Peng, "The North American multimodel ensemble: Phase-1 seasonal-to-interannual prediction; phase-2 toward developing intraseasonal prediction," *Bull. Amer. Meteorol. Soc.*, vol. 95, no. 4, pp. 585–601, Apr. 2014, doi: 10.1175/bams-d-12-00050.1.
[47] O. Boucher, S. Denvil, G. Levavasseur, A. Cozic, A. Caubel, M. A. Foujols, Y. Meurdesoif, P. Cadule, M. Devilliers, J. Ghattas, N. Lebas, T. Lurton, L. Mellul, I. Musat, J. Mignot, and F. Cheruy. (Jan. 1, 2018). *CMIP6.CMIP.IPSL.IPSL-CM6A-LR.Historical*, doi: 10.22033/esgf/cmip6.5195.
[48] H. Pohlmann, M. Schupfner, K. H. Wieners, F. Wachsmann, C. Steger, M. Bittner, J. Jungclaus, B. Früh, K. Pankatz, M. Giorgetta, and C. Reick. (Jan. 1, 2019). *CMIP6.CMIP.MPI-M.MPI-ESM1-2-HR.Historical*, doi: 10.22033/esgf/cmip6.6594.
[49] D. Neubauer, S. Ferrachat, C. Siegenthaler-Le Drian, J. Stoll, D. S. Folini, I. Tegen, and U. Lohmann. (Jan. 1, 2019). *CMIP6.CMIP.HAMMOZ-Consortium.MPI-ESM-1-2-HAM.Historical*, doi: 10.22033/esgf/cmip6.5016.
[50] EC-Earth Consortium (EC-Earth), (2019), "EC-Earth-Consortium EC-Earth3 model output prepared for CMIP6 CMIP historical," *Earth System Grid Federation*, doi: 10.22033/ESGF/CMIP6.4700.
[51] T. Lovato and D. Peano, (2020), "CMCC CMCC-CM2-SR5 model output prepared for CMIP6 CMIP historical," *Earth System Grid Federation*, doi: 10.22033/ESGF/CMIP6.3825.
[52] D. W. Behringer, M. Ji, and A. Leetmaa, "An improved coupled model for ENSO prediction and implications for ocean initialization. Part I: The ocean data assimilation system," *Monthly Weather Rev.*, vol. 126, no. 4, pp. 1013–1021, Apr. 1998, doi: 10.1175/1520-0493(1998)126<1013:AICMFE>2.0.CO;2.
[53] J. A. Carton and B. S. Giese, "A reanalysis of ocean climate using simple ocean data assimilation (SODA)," *Monthly Weather Rev.*, vol. 136, no. 8, pp. 2999–3017, Aug. 2008, doi: 10.1175/2007mwr1978.1.
[54] R. W. Reynolds, N. A. Rayner, T. M. Smith, and D. C. Stokes, "An improved in situ and satellite SST analysis for climate," *J. Climate*, vol. 15, no. 13, pp. 1609–1625, Jul. 2002, doi: 10.1175/1520-0442(2002)015<1609:AIISAS>2.0.CO;2.
[55] Y. Lecun, L. Bottou, Y. Bengio, and P. Haffner, "Gradient-based learning applied to document recognition," *Proc. IEEE*, vol. 86, no. 11, pp. 2278–2324, Jan. 1998, doi: 10.1109/5.726791.
[56] S. Ji, W. Xu, M. Yang, and K. Yu, "3D convolutional neural networks for human action recognition," *IEEE Trans. Pattern Anal. Mach. Intell.*, vol. 35, no. 1, pp. 221–231, Jan. 2013, doi: 10.1109/TPAMI.2012.59.
[57] P. Chen, B. Sun, H. Wang, and L. Yang, "Improving the CFSv2 prediction of the Indian ocean dipole based on a physical-empirical model and a deep-learning approach," *Int. J. Climatol.*, vol. 42, no. 16, pp. 9200–9214, Aug. 2022, doi: 10.1002/joc.7812.
[58] P. P. Sarkar, P. Janardhan, and P. Roy, "A novel deep neural network model approach to predict Indian ocean dipole and equatorial Indian ocean oscillation indices," *Dyn. Atmos. Oceans*, vol. 96, Dec. 2021, Art. no. 101266, doi: 10.1016/j.dynatmoce.2021.101266.
[59] C. Li, Y. Feng, T. Sun, and X. Zhang, "Long term Indian ocean dipole (IOD) index prediction used deep learning by convLSTM," *Remote Sens.*, vol. 14, no. 3, p. 523, Jan. 2022, doi: 10.3390/rs14030523.
[60] Y. Yu, M. Yao, J. Huang, and X. Xiao, "When process analysis technology meets transfer learning: A model transfer strategy between different spectrometers for quantitative analysis," *IEEE Trans. Instrum. Meas.*, vol. 73, pp. 1–19, 2024, doi: 10.1109/TIM.2024.3353273.
[61] Y. Yu and M. Yao, "When convolutional neural networks meet laser-induced breakdown spectroscopy: End-to-end quantitative analysis modeling of ChemCam spectral data for major elements based on ensemble convolutional neural networks," *Remote Sens.*, vol. 15, no. 13, p. 3422, Jul. 2023, doi: 10.3390/rs15133422.

MANVENDRA JANMAIJAYA (Graduate Student Member, IEEE) received the B.Sc. degree (Hons.) in computer science from the University of Delhi, India, in 2012, the M.Sc. degree in computer science from South Asian University (SAU), New Delhi, India, in 2014, and the Master of Technology degree in computer science engineering from Gautam Buddha University, Greater Noida, India, in 2016. He is currently pursuing the Ph.D. degree with the Department of Computer Science, South Asian University. His current research interests include neural networks, machine learning, and scientometrics.

MANSI JANMAIJAYA received the Ph.D. degree in geography from the University of Delhi, New Delhi, India, in 2021.

She is currently an Assistant Professor with the Department of Geography, K. G. K. (PG) College, Moradabad, India. Her current research interests include climate variability and change, meteorology, climate vulnerability, climate adaptation, and climate justice. She was a recipient of the Junior and Seniors Research Fellowships awarded by the Government of India for the Ph.D. degree.

PRANAB K. MUHURI (Senior Member, IEEE) was born in Chattogram, Bangladesh. He received the Ph.D. degree in computer engineering from IT-BHU [now, Indian Institute of Technology (BHU)], Varanasi, India, in 2005.

He is currently a Professor with the Department of Computer Science, South Asian University, New Delhi, India, where he is leading the Computational Intelligence Research Group. He has published more than 100 papers in reputed journals and conferences, including IEEE TRANSACTIONS ON FUZZY SYSTEMS, IEEE TRANSACTIONS ON CYBERNETICS, IEEE TRANSACTIONS ON SUSTAINABLE COMPUTING, *Reliability Engineering and System Safety*, *Fuzzy Sets and Systems*, *Applied Soft Computing*, *Computers and Industrial Engineering*, *Ecological Informatics*, and *Future Generation Computer Systems*. His current research interests include real-time systems, fuzzy systems, evolutionary algorithms, perceptual computing, and machine learning. He has been serving as an Editorial Board Member for journals, such as *Applied Soft Computing* and *Engineering Applications of Artificial Intelligence*.